GSA Data Repository 2020043

Cui, H., et al., 2020, Forming sulfate- and REE-rich fluids in the presence of quartz: Geology, v. 48, https://doi.org/10.1130/G46893.1

Supplementary material

Material and methods

Reagents preparation. Analytical grade solid Na_2SO_4 (>99.0%), solid $Nd_2(SO_4)_3 \cdot 8H_2O$ (99.9%), $Na_2SO_4 \cdot 10H_2O$ (mirabilite), and deionized water were used as starting materials and for preparation of sulfate-saturated solution. Gem-grade quartz crystal from Donghai in eastern China was used. The quartz crystal was crushed and milled in a mortar for 20 minutes to reduce the grain sizes to ~100 μm.

HDAC apparatus and experiment conduction. An HDAC (Bassett et al., 1996) was used for the experiments. Two opposed low-fluorescence diamond anvils with 1 mm diameter culets were seated upon a tungsten carbide seat respectively. The anvils were heated by two nickel-chromium heaters wound around the seats to subject the samples to high P-T condition (up to 550 °C). The sample chamber was sealed by compressing the two diamond anvils against a 400 μm diameter hole in the center of a 200 μm thick Re gasket. Temperature inside the sample chamber was measured by two K-type thermocouples attached to each of the diamond anvils, calibrated by measuring the melting points of native sulfur (112 °C) and sodium nitrate (307 °C) (Yuan et al., 2016). Heating rate was controlled at <2 °C/min near phase transitions. Quartz was used as a Raman spectroscopic pressure sensor, with pressure uncertainty of about ±50 MPa (Schmidt and Ziemann, 2000).

Sulfate(s) and water were loaded into the sample chamber in four methods: (i) loading Na_2SO_4 crystal(s) and then Na_2SO_4-saturated water solution; (ii) loading only mirabilite to quantify the

Na_2SO_4/H_2O ratio; (iii) loading mirabilite and Na_2SO_4 piece(s) to get bulk compositions with Na_2SO_4/H_2O ratios >0.1; and (iv) loading mirabilite and $Nd_2(SO_4)_3 \cdot 8H_2O$ to investigate Nd solubility in sulfate-rich solution. To prevent mirabilite from dehydrate (up to 32.4 °C), it was loaded at ~−30 °C in a refrigerator. HDAC and Re gaskets were also kept in the refrigerator for at least 20 minutes before sample loading, to make sure that mirabilite would not "melt" on the warm anvils.

The Re gaskets were one-time use and repeated heating and cooling of the samples was avoided to minimize reactions between sulfate and Re gasket. The major effect of this reaction is a decrease in the fluid sulfate concentration. Electronic microscopic observation shows that trace amounts of Re-sulfide was generated, but can be neglected compared to the very high bulk sulfate contents of the system. Minor changes in the fluid redox might also happen, but it would not influence the phase relationships.

Gold-lined gaskets were used for experiments with repeating heating and cooling (results shown in Fig. 1), to avoid reaction between fluid and Re gaskets. The gold-lined gasket was made by filling metallic gold in the hole of the Re gasket and then drilling a smaller (~300 μm diameter) hole in the center.

The phase diagram of Figure 1 was constituted by results of five runs of experiments with the same bulk Na_2SO_4/H_2O ratio. One run of the experiments was carried using gold-line gasket while others using common Re gasket. The phase diagram shows consistent P- and T-dependences of phase boundaries, suggesting that the bulk compositions of the five runs remained nearly identical and unchanged during heating, i.e., limited degree of fluid-Re reaction.

After the experiments of the silica-bearing systems, a pair of new diamond anvils was used for

the quartz-absent "blank control" experiments (Fig. DR2). The anvils were carefully washed in HF solution (10 wt.%) to avoid any contamination by silica.

Raman spectra acquisition and processing. The Raman spectra were acquired using a HORIBA Jobin Yvon confocal LabRAM HR Evolution micro-Raman system installed at Peking University. The system is equipped with a frequency doubled Nd:YAG green laser (532.06 nm), a 20× long-working distance objective with 0.25 numerical aperture, and a stigmatic 800 mm spectrometer with a 1800 groove/mm grating. The laser power was 100 mW at the source. The confocal hole was set at 500 μm and the corresponding spectral resolution was ±0.7 cm^{-1}. During the experiments, Raman spectra between 100 and 1300 cm^{-1} were recorded, with a continuing time of 10 and 15 seconds for sodium sulfate and quartz, respectively.

An external light source generated by a Philips 8-watt fluorescent lamp was used as a standard (at 1463 cm^{-1} for the 532.06 nm laser) to calibrate the spectroscopy drift during the experiments (Yuan et al., 2016). The spectra of the fluorescent lamp were collected after the acquisitions of each quartz spectra (Lu et al., 2007; Scott et al., 2004). The calibrated Raman positions (ν_{corr}) of quartz were calculated from Raman band value ($\nu_{measured}$) using the following relationship:

$$\nu_{corr}\ (cm^{-1}) = \nu_{measured} - \nu_{l} + \nu_{l,\ standard}$$

where $\nu_{measured}$ denotes the measured Raman position of quartz, and ν_{l} is the position of lamp fluorescence collected after each quartz spectra, and $\nu_{l,standard}$ is that of lamp fluorescence that was collected at the beginning of each run of HDAC experiment. The Peakfit 4.0 package of the SYSTAT Software Inc. was used to process the Raman spectra. The peaks of sodium sulfate, quartz and fluorescent lamp were all fitted with Pearson IV amplify functions because of the asymmetric properties of those peaks (Yuan and Mayanovic, 2017).

Scanning electron microscopic observation. Quenched sulfate melt attached to the Re gasket was collected after the HDAC experiment and coated with gold. The sulfate was observed and compositionally analyzed using the Phenom XL benchtop scanning electron microscope with an accelerating potential of 15 kV at the Civil and Resource Engineering School of University of Science and Technology Beijing.

Thermodynamic modeling. The thermodynamic modeling was carried out using the HCh program (Bastrakov, 1999). Activity coefficients for charged aqueous species were calculated using the b-dot equation (Bastrakov, 1999; Helgeson and Kirkham, 1974), and those for neutral species were unit. The simulations were performed by calculating the full speciation of solutions that are saturated in fluorite, fluorapatite, calcite, and monazite-(Nd) and contains 5 molal of dissolved CO_2, 2 molal of NaCl, and 2 molal of Na_2SO_4 from 300 to 500 °C at 150 MPa. In the quartz-absent simulation, solid Na_2SO_4(s) and $Nd_2(SO_4)_3$(s) are included in the model, and therefore the retrograde solubility can be reproduced via the precipitation of the solids at high temperatures.

The interaction between silica and sulfate ion cannot be directly simulated due to the lack of available thermodynamic data. The immediate consequence of the presence of quartz is an elevation in the solubility of sulfate salts, and the quartz-saturated experiment (Fig. 2) shows that the high-temperature (300 to 500 °C) solubility of Na_2SO_4(s) and $Nd_2(SO_4)_3$(s) are much higher than the concentrations of dissolved sulfate (2 molal) and Nd (up to ~50 ppm), although the experiment is not quantitative. Therefore, the elevated sulfate solubility in the presence of quartz can be simulated simply be removing sulfate solids from the system and sulfate in the system was thus forced to be fluid-borne through the whole temperature range. This simple approach cannot precisely reproduce the silica-sulfate interaction but can simulate the elevated sulfate

concentration, which has the first-order control in the hydrothermal speciation and mobility of REE(III). Thermodynamic properties used in the simulation are listed in Table DR2.

Experimental details

Confirmation of sulfate melting by optical observation. In some cases, especially at the beginning stages of melting, the molten sulfate can hardly be distinguished from sulfate solid by the appearance. In these scenarios, the phenomenon that two sulfate melt droplets merges into a single bigger drop (Fig. DR3) provide a solid evidence for the liquid state of the sulfate.

Confirmation of incipient melting of sulfate. The coupling between incipient melting and the transition from Type III to I polymorphs is evidenced by the presence of amorphous sulfate in samples that was quenched shortly after the solid-solid phase transition (Fig. DR4). The quenching was done in a dry state, as described in the main text.

Confirmation of the equilibrium of the experimental system. To evaluate whether the phase relationship shown in Figure 1 is stable or metastable, one run of experiment using gold-lined gasket and mirabilite and quartz as starting materials was carried out and the heating and cooling cycle was repeated three times. Upon heating, the reproducibility of the measured solidus and total homogenization temperature is within ± 2 °C. We therefore conclude that the phase boundaries determined during heating represent stable assemblages. Metastable assemblages (supercooling) occur over a narrow temperature range during cooling. For example, the homogenization temperatures obtained during the three runs of cooling (i.e., exsolution of the melt) are in overall ~20 °C lower than that determined during heating.

REFERENCES CITED

Akinfiev, N., 1998, Speciation and mineral equilibria in the mixed natural fluids H_2O-non polar gas: Mineralogical Magazine, v. 62, no. 1, p. 25–26.

Bassett, W. A., Wu, T. C., Chou, I. M., Jr Haselton, H. T., Frantz, J. D., Mysen, B. O., Huang, W. L., Sharma, S. K., and Schifer, L. D., 1996, The hydrothermal diamond anvil cell (HyDAC) and its applications: Special Publication: Geochemical Society, v. 5, p. 261–272.

Bastrakov, E. N., 1999, HCh: a software package for geochemical equilibrium modelling. User's guide.

Berman, R. G., 1988, Internally-consistent thermodynamic data for minerals in the system Na_2O-K_2O-CaO-MgO-FeO-Fe_2O_3-Al_2O_3-SiO_2-TiO_2-H_2O-CO_2: Journal of Petrology, v. 29, no. 2, p. 445–522.

Haas, J. R., Shock, E. L., and Sassani, D. C., 1995, Rare earth elements in hydrothermal systems: Estimates of standard partial molal thermodynamic properties of aqueous complexes of the rare earth elements at high pressures and temperatures: Geochimica et Cosmochimica Acta, v. 59, no. 21, p. 4329–4350.

Helgeson, H. C., and Kirkham, D. H., 1974, Theoretical prediction of the thermodynamic behavior of aqueous electrolytes at high pressures and temperatures; II, Debye-Huckel parameters for activity coefficients and relative partial molal properties: American Journal of Science, v. 274, no. 10, p. 53.

Johnson, J. W., Oelkers, E. H., and Helgeson, H. C., 1992, SUPCRT92: A software package for calculating the standard molal thermodynamic properties of minerals, gases, aqueous species, and reactions from 1 to 5000 bars and 0 to 1000 °C, Computers and Geosciences, v. 18, no. 1,

p. 899–947.

Kestin, J., Sengers, J. V., Kamgarparsi, B., and Sengers, J. M. H. L., 1984, Thermophysical properties of fluid D_2O: Journal of Physical & Chemical Reference Data, v. 13, no. 1, p. 175–183.

Knacke, O., Kubaschewski, O., and Hesselman, K., 1991, Thermochemical properties of inorganic substances, 2nd ed: Springer-Verlag, Berlin, p. 1113.

Lu, W. J., Chou, I. M., Burruss, R. C., and Song, Y. C., 2007, A unified equation for calculating methane vapor pressures in the CH_4-H_2O system with measured Raman shifts: Geochimica et Cosmochimica Acta, v. 71, no. 16, p. 3969–3978.

Malinin, A. A., 1983, Study of the dynamic characteristics of thin-walled structures with attached weights: Soviet Applied Mechanics, v. 19, no. 2, p. 147–149.

Marshall, W. L., and Franck, E. U., 1981, Ion product of water substance, 0-1000 ˚C, 1-10000 bars: new international formulation and its background: Journal of Physical & Chemical Reference Data, v. 10, p. 10.

Migdisov, A. A., Reukov, V. V., and Williams-Jones, A. E., 2006, A spectrophotometric study of neodymium(III) complexation in sulfate solutions at elevated temperatures: Geochimica et Cosmochimica Acta, v. 70, no. 4, p. 983–992.

Migdisov, A. A., Williams-Jones, A. E., and Wagner, T., 2009, An experimental study of the solubility and speciation of the Rare Earth Elements (III) in fluoride- and chloride-bearing aqueous solutions at temperatures up to 300 °C: Geochimica et Cosmochimica Acta, v. 73, no. 23, p. 7087–7109.

Murugan, R., Ghule, A., and Chang, H., 2000, Thermo-Raman spectroscopic studies on polymorphism in Na_2SO_4: Journal of Physics-Condensed Matter, v. 12, no. 5, p. 677–700.

Plyasunov, A. V., and Shock, E. L., 2001, Correlation strategy for determining the parameters of the revised Helgeson-Kirkham-Flowers model for aqueous nonelectrolytes: Geochimica et Cosmochimica Acta, v. 65, no. 21, p. 3879–3900.

Pokrovski, G. S., and Dubessy, J., 2015, Stability and abundance of the trisulfur radical ion S_3^- in hydrothermal fluids: Earth and Planetary Science Letters, v. 411, p. 298–309.

Pokrovski, G. S., Schott, J., and Sergeyev, A. S., 1995, Experimental determination of the stability constants of $NaSO_4^-$ and $NaB(OH)_4^0$ in hydrothermal solutions using a new high-temperature sodium-selective glass electrode – Implications for boron isotopic fractionation: Chemical Geology, v. 124, no. 3, p. 253–265.

Pokrovski, V. A., 1998, ETHZ version of SUPCRT.

Popa, K., and Konings, R. J. M., 2006, High-temperature heat capacities of $EuPO_4$ and $SmPO_4$ synthetic monazites: Thermochimica Acta, v. 445, no. 1, p. 49–52.

Robie, R. A., Hemmingway, B. S., and Fisher, J. R., 1979, Thermodynamic properties of minerals and related substances at 298.15 K and 1 bar pressure and at higher temperature: US Geological Survey Bulletin 1452, US Government Printing Office, Washington, p. 456.

Rudolph, W. W., Brooker, M. H., and Tremaine, P. R., 1999, Raman spectroscopy of aqueous $ZnSO_4$ solutions under hydrothermal conditions: Solubility, hydrolysis, and sulfate ion pairing: Journal of Solution Chemistry, v. 28, no. 5, p. 621–630.

Schmidt, C., and Ziemann, M. A., 2000, In-situ Raman spectroscopy of quartz: A pressure sensor for hydrothermal diamond-anvil cell experiments at elevated temperatures: American Mineralogist, v. 85, no. 11–12, p. 1725–1734.

Scott, J. G., Mailis, S., Sones, C. L., and Eason, R. W., 2004, A Raman study of single-crystal

congruent lithium niobate following electric-field repoling: Applied Physics a-Materials Science & Processing, v. 79, no. 3, p. 691–696.

Shock, E. L., and Helgeson, H. C., 1988, Calculation of the thermodynamic and transport properties of aqueous species at high pressures and temperatures: Correlation algorithms for ionic species and equation of state predictions to 5 kb and 1000 °C: Geochimica et Cosmochimica Acta, v. 52, no. 8, p. 2009–2036.

Shock, E. L., Sassani, D. C., Willis, M., and Sverjensky, D. A., 1997, Inorganic species in geologic fluids: Correlations among standard molal thermodynamic properties of aqueous ions and hydroxide complexes: Geochimica et Cosmochimica Acta, v. 61, no. 5, p. 907–950.

Smith, R. M., and Martell, A. E., 1976, Critical stability constants: inorganic complexes: New York, Plenum Press.

Sverjensky, D. A., Shock, E. L., and Helgeson, H. C., 1997, Prediction of the thermodynamic properties of aqueous metal complexes to 1000 °C and 5 kbars: Geochimica et Cosmochimica Acta, v. 61, no. 7, p. 1359–1412.

Tagirov, B. R., Zotov, A. V., and Akinfiev, N. N., 1997, Experimental study of dissociation of HCl from 350 to 500 °C and from 500 to 2500 bars: Thermodynamic properties of HCl° (aq): Geochimica et Cosmochimica Acta, v. 61, no. 61, p. 4267–4280.

Wood, S., Palmer, D., Wesolowski, D., and Bénézeth, P., 2002, The aqueous geochemistry of the rare earth elements and yttrium. Part XI. The solubility of $Nd(OH)_3$ and hydrolysis of Nd^{3+} from 30 to 290 °C at saturated water vapor pressure with in-situ pHm measurement.: Water-Rock Interactions, Ore Deposits, and Environmental Geochemistry: A Tribute to David A, v. 7, no. 28, p. 229–256

Yuan, X., and Mayanovic, R. A., 2017, An empirical study on Raman peak fitting and its application to Raman quantitative research: Applied Spectroscopy, v. 71, no. 10, p. 2325–2338.

Yuan, X. Y., Mayanovic, R. A., and Zheng, H. F., 2016, Determination of pressure from measured Raman frequency shifts of anhydrite and its application in fluid inclusions and HDAC experiments: Geochimica et Cosmochimica Acta, v. 194, p. 253–265.

Supplementary figures

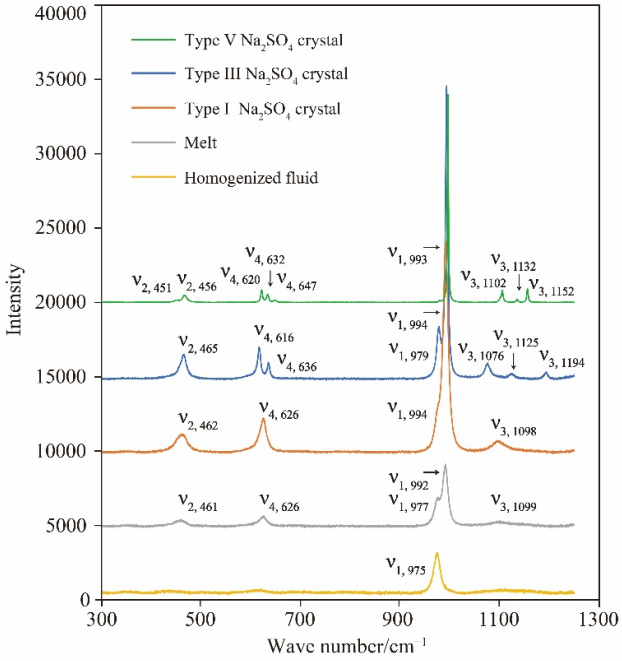

Figure DR1. Raman spectroscopy for different sulfate phases. Three polymorphs of solid Na_2SO_4 (Type V, III and I) were recognized by Raman spectroscopy (Murugan et al., 2000). Type V crystal is characterized by two sub-peaks of ν_2 located at 451 cm^{-1} and 456 cm^{-1} and triplet for ν_3 located at 1102 cm^{-1}, 1132 cm^{-1} and 1152 cm^{-1}, respectively. Type III crystal also has a triplet for ν_3, but the sub-peaks are different from those of Type V. Type I crystal is characterized by a singlet for ν_3 at 1098 cm^{-1}. Sulfate melt has weaker and broader peaks compared to the crystal counterparts with subpeaks at 992 and 997 cm^{-1}, which are vibrations of monodentate Na^+-SO_4^{2-} ion pair or polymer and free sulfate ion SO_4^{2-}, respectively (Rudolph et al., 1999). The spectroscopy for homogenized fluid only has a main peak at 975 cm^{-1}, the signal of free SO_4^{2-} (Rudolph et al., 1999).

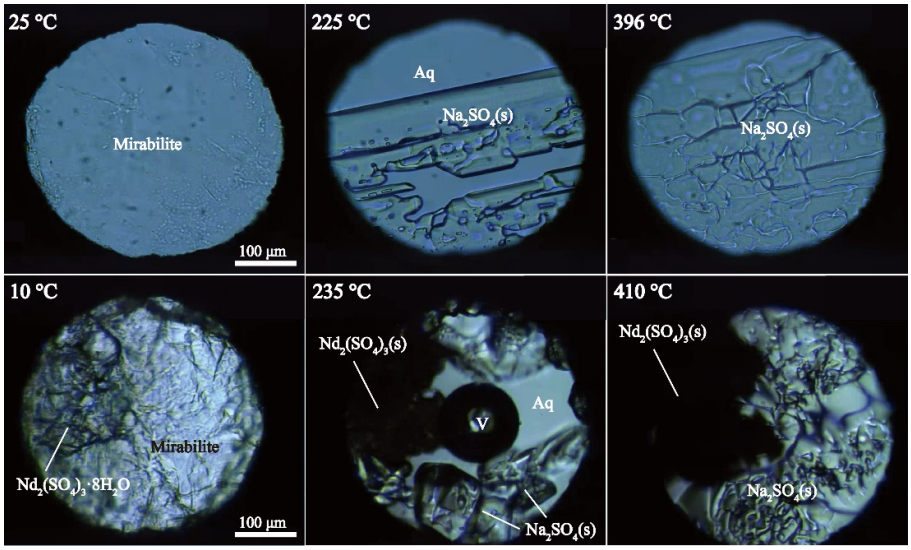

213

214 **Figure DR2. HDAC results of the Na_2SO_4-H_2O (top) and Na_2SO_4-$Nd_2(SO_4)_3$-H_2O (bottom) systems.** In the

215 absence of quartz, sulfates are characterized by retrograde solubility. Mirabilite and $Nd_2(SO_4)_3 \cdot 8H_2O$ were loaded as

216 starting materials.

217

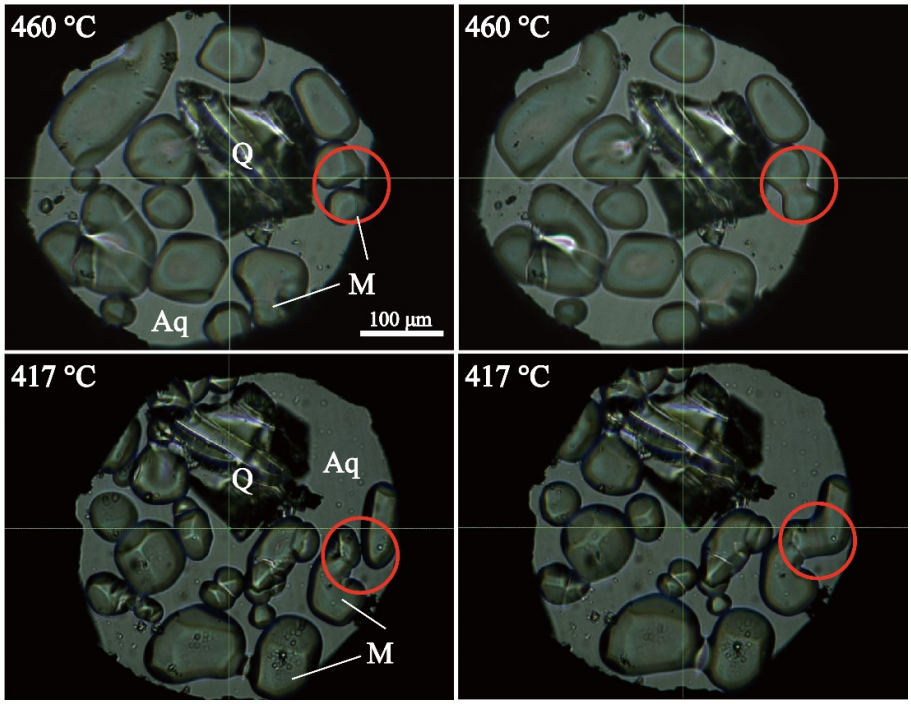

218

219 **Figure DR3. Merging of sulfate droplets observed at 460 and 417 °C, respectively.** Na_2SO_4 crystal,

220 Na_2SO_4-saturated solution and quartz were loaded as starting materials.

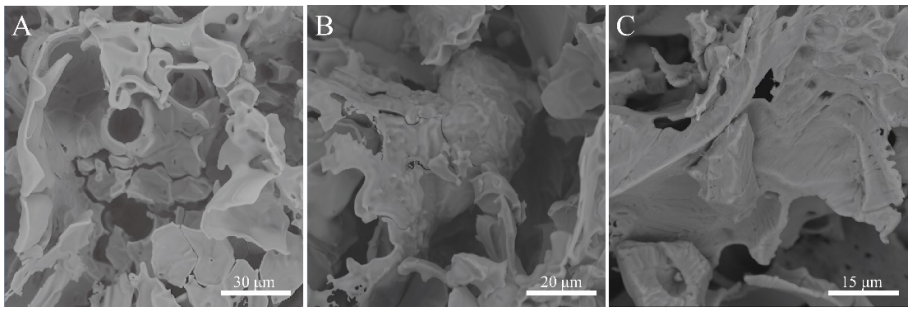

Figure DR4. Backscattered electron images of amorphous sulfate from samples that were quenched shortly after the Type III to I phase transition.

Supplementary table

Table DR1. Phase transition boundaries determined from three runs of experiments with Na_2SO_4/H_2O molar ratio >0.1. The experiments were conducted using gold-lined Re gaskets.

	Phase III to I (solidus)	Total homogenization
Round 1	267 °C, 257 MPa	434 °C, 573 MPa
Round 2	260 °C, 253 MPa	450 °C, 753 MPa
Round 3	280 °C, 132 MPa	397 °C, 494 MPa

Table DR2. Solid and aqueous species used in the modeling and sources of thermodynamic properties.

Species	Formula/Equation of states	Reference
Solids		
Fluorite	CaF_2	Robie et al., 1979
Calcite	$CaCO_3$	Berman, 1988
Monazite-(Nd)	$NdPO_4$	Popa and Konings, 2006
$Na_2SO_4(s)$	Na_2SO_4	Knacke et al., 1991
$Nd_2(SO_4)_3(s)$	$Nd_2(SO_4)_3$	Knacke et al., 1991
$NdF_3(s)$	NdF_3	Knacke et al., 1991
OH-apatite	$Ca_5(PO_4)_3OH$	Robie et al., 1979
Aqueous species		
H_2O		Kestin et al., 1984
H^+		Marshall and Franck, 1981
OH^-		Marshall and Franck, 1981
$H_2(aq)$	Revised HKF	Johnson et al., 1992
$O_2(aq)$	Revised HKF	Johnson et al., 1992
$CH_4(aq)$	Revised HKF	HCh build-in (Unitherm) (Bastrakov, 1999)
CO_3^{2-}	Revised HKF	Johnson et al., 1992
HCO_3^-	Revised HKF	Johnson et al., 1992
$CO_2(aq)$	Revised HKF	HCh build-in (Unitherm) (Bastrakov, 1999)
PO_4^{3-}	Revised HKF	HCh build-in (Unitherm) (Bastrakov, 1999)

$H_2PO_4^-$	Revised HKF	HCh build-in (Unitherm) (Bastrakov, 1999)
HPO_4^{2-}	Revised HKF	HCh build-in (Unitherm) (Bastrakov, 1999)
H_3PO_4(aq)	Revised HKF	HCh build-in (Unitherm) (Bastrakov, 1999)
S_2^{2-}	Revised HKF	Johnson et al., 1992
HS^-	Revised HKF	Shock and Helgeson, 1988
H_2S(aq)	Revised HKF	Plyasunov and Shock, 2001
$S_2O_3^{2-}$	Revised HKF	Johnson et al., 1992
$HS_2O_3^-$	Revised HKF	Shock et al., 1997
$H_2S_2O_3$(aq)	Revised HKF	Shock et al., 1997
SO_2(aq)	Revised HKF	Johnson et al., 1992
SO_3^{2-}	Revised HKF	Johnson et al., 1992
HSO_3^-	Revised HKF	Johnson et al., 1992
SO_4^{2-}	Revised HKF	Johnson et al., 1992
HSO_4^-	Revised HKF	Johnson et al., 1992
S^{3-}	Revised HKF	Pokrovski and Dubessy., 2015
F^-	Revised HKF	HCh build-in (Unitherm) (Bastrakov, 1999)
HF(aq)	Revised HKF	HCh build-in (Unitherm) (Bastrakov, 1999)
HF_2^-	MRB model	Malinin 1983
Cl^-	Revised HKF	Shock et al., 1997
HCl(aq)	Revised HKF	Tagirov et al., 1997
Na^+	Revised HKF	Johnson et al., 1992
NaOH(aq)	Revised HKF	SUPCRT95 (Pokrovski, 1998)

NaCl(aq)	Revised HKF	Sverjensky et al., 1997
NaF(aq)	Revised HKF	SUPCRT95 (Pokrovski, 1998)
NaHS(aq)	MRB model	Calculated from the assumption: pK(NaHS) = pK(NaCl)
$NaCO_3^-$	MRB model	Smith and Martell 1976
$NaHCO_3$(aq)	MRB model	Smith and Martell 1976
$NaSO_4^-$	Revised HKF	Pokrovski et al., 1995
Ca^{2+}	Revised HKF	HCh build-in (Unitherm) (Bastrakov, 1999)
$CaOH^+$	Revised HKF	Akinfiev 1998
CaF^+	MRB model	Malinin 1983
$CaCl^+$	Revised HKF	SUPCRT95 (Pokrovski, 1998)
$CaCl_2$(aq)	Revised HKF	SUPCRT95 (Pokrovski, 1998)
$CaCO_3$(aq)	Revised HKF	SUPCRT95 (Pokrovski, 1998)
$Ca(HCO_3)^+$	Revised HKF	Akinfiev 1998
$CaSO_4$(aq)	Revised HKF	SUPCRT95 (Pokrovski, 1998)
Nd^{3+}	Revised HKF	Shock and Helgeson, 1988
$NdCO_3^+$	Revised HKF	Haas et al., 1995
$NdHCO_3^{2+}$	Revised HKF	Haas et al., 1995
$NdH_2PO_4^{2+}$	Revised HKF	Haas et al., 1995
$NdSO_4^+$	MRB mode	Migdisov et al., 2006
$Nd(SO_4)_2^-$	MRB mode	Migdisov et al., 2006
$NdOH^{2+}$	MRB mode	Wood et al., 2002

$Nd(OH)_2^+$	MRB mode	Wood et al., 2002
$Nd(OH)_3(aq)$	MRB mode	Wood et al., 2002
NdF^{2+}	Revised HKF	Migdisov et al., 2009
$NdCl^{2+}$	Revised HKF	Migdisov et al., 2009
$NdCl_2^+$	Revised HKF	Migdisov et al., 2009

238

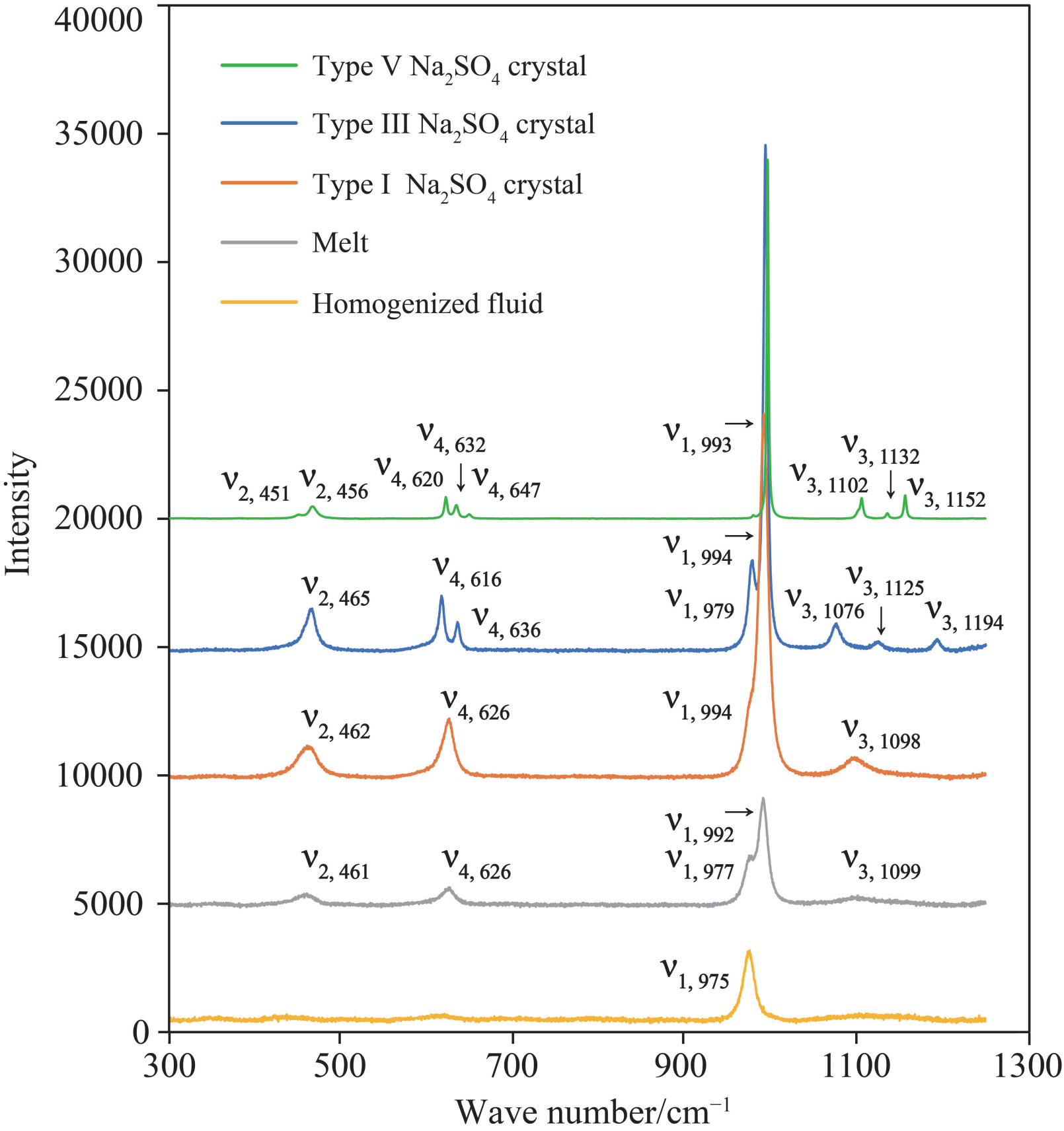
Type V Na_2SO_4 crystal
Type III Na_2SO_4 crystal
Type I Na_2SO_4 crystal
Melt
Homogenized fluid
Intensity
Wave number/cm^{-1}
40000
35000
30000
25000
20000
15000
10000
5000
0
300
500
700
900
1100
1300
$\nu_{2, 451}$
$\nu_{2, 456}$
$\nu_{4, 620}$
$\nu_{4, 632}$
$\nu_{4, 647}$
$\nu_{1, 993}$
$\nu_{3, 1102}$
$\nu_{3, 1132}$
$\nu_{3, 1152}$
$\nu_{2, 465}$
$\nu_{4, 616}$
$\nu_{4, 636}$
$\nu_{1, 994}$
$\nu_{1, 979}$
$\nu_{3, 1076}$
$\nu_{3, 1125}$
$\nu_{3, 1194}$
$\nu_{2, 462}$
$\nu_{4, 626}$
$\nu_{1, 994}$
$\nu_{3, 1098}$
$\nu_{2, 461}$
$\nu_{4, 626}$
$\nu_{1, 992}$
$\nu_{1, 977}$
$\nu_{3, 1099}$
$\nu_{1, 975}$

Fig. DR1

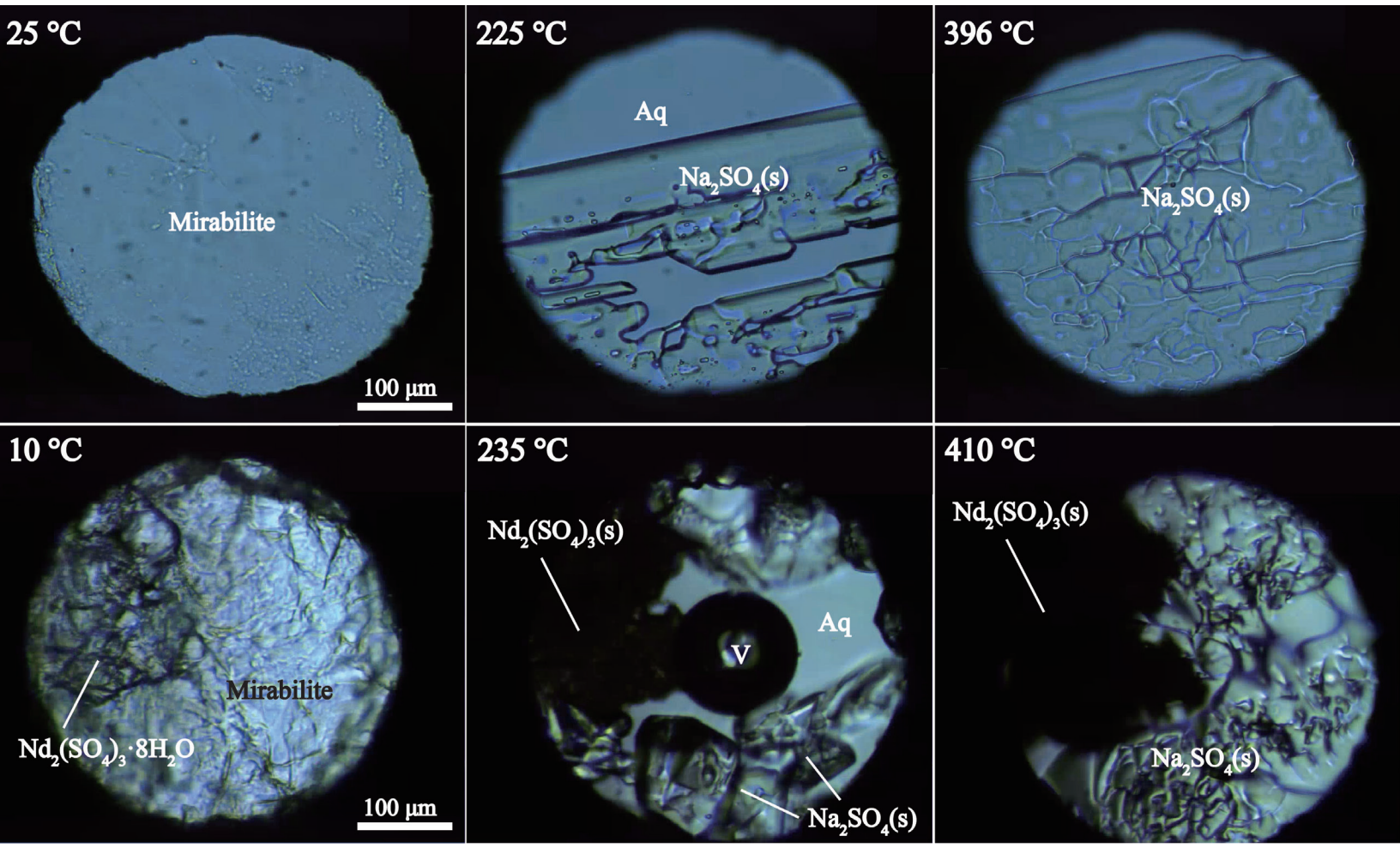
25 °C
Mirabilite
100 µm
225 °C
Aq
Na_2SO_4(s)
396 °C
Na_2SO_4(s)
10 °C
Mirabilite
$Nd_2(SO_4)_3 \cdot 8H_2O$
100 µm
235 °C
$Nd_2(SO_4)_3$(s)
Aq
V
Na_2SO_4(s)
410 °C
$Nd_2(SO_4)_3$(s)
Na_2SO_4(s)

Fig. DR2

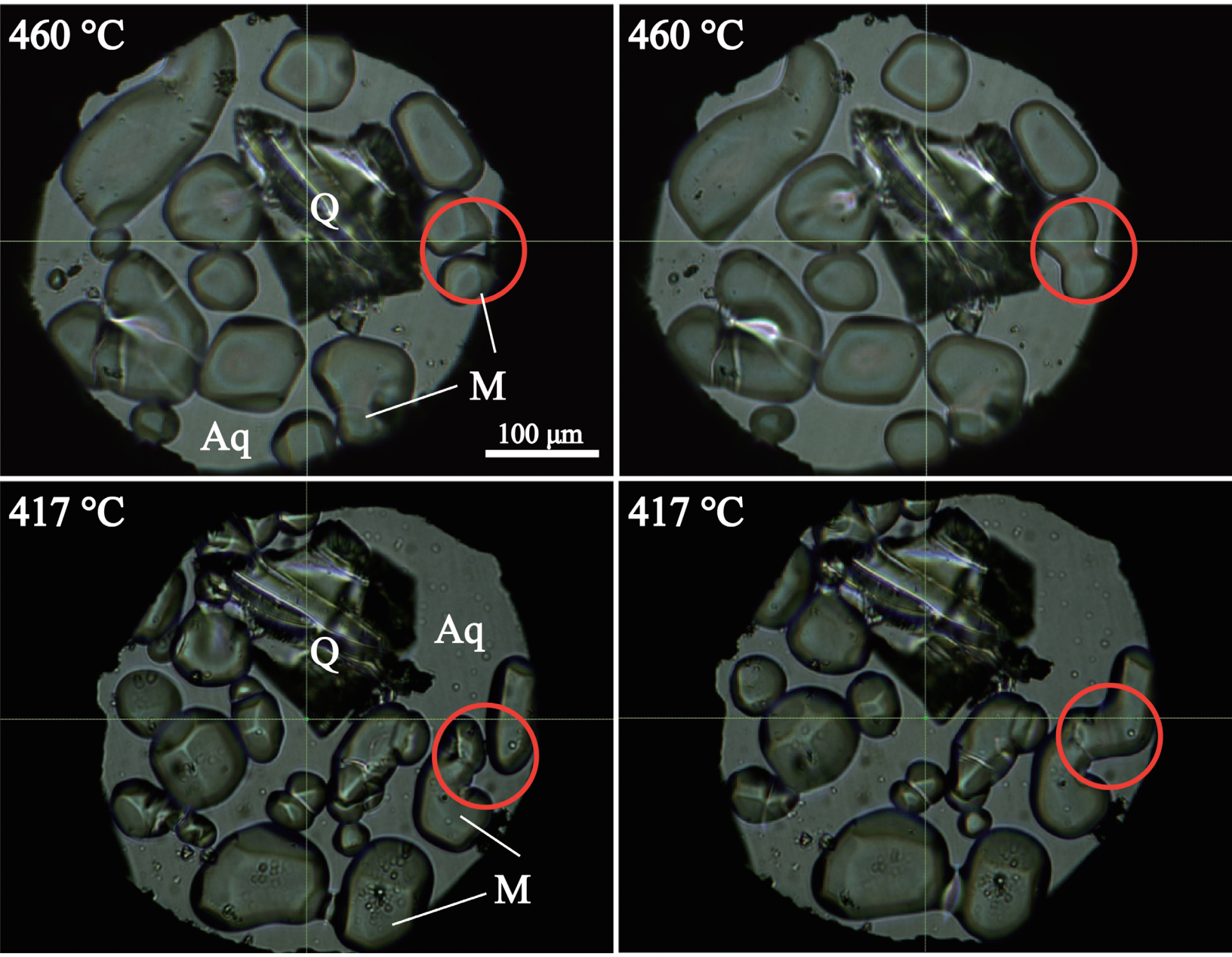

Fig. DR3

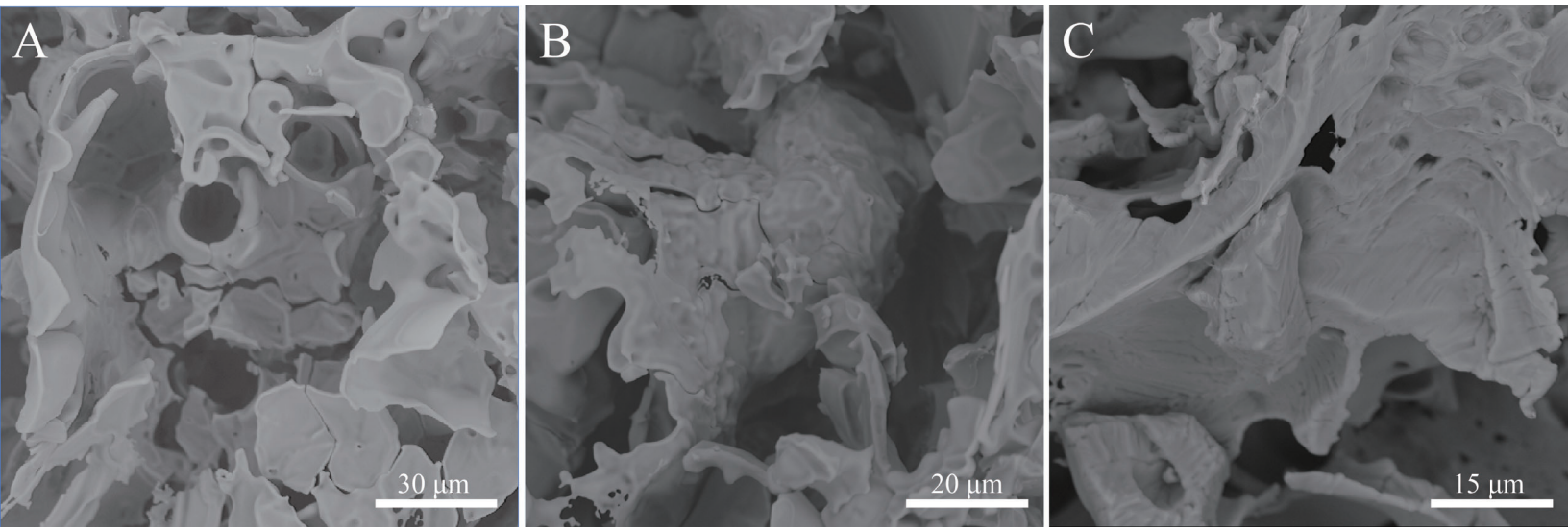

Fig. DR4